

## Supporting Information

Structure and properties of naphthalene-diimide N-functionalized with stilbene

A. Yu. Sosorev<sup>1,2\*</sup>, I. I. Ponomarev<sup>3</sup>, D. I. Dominskiy<sup>1,2</sup>, K. A. Lyssenko<sup>3</sup>, O. D. Parashchuk<sup>1</sup>, V. A. Trukhanov<sup>1,2</sup>, V.G. Konstantinov<sup>1,2</sup>, N.O. Dubinets<sup>4</sup>, D. Yu. Paraschuk<sup>1,2</sup>.

1. Faculty of Physics, Lomonosov Moscow State University, Leninskie Gory 1/62, Moscow 119991, Russia

2. Enikolopov Institute of Synthetic Polymeric Materials, Russian Academy of Science, Profsoyuznaya 70, Moscow 117393, Russia

3. A.N. Nesmeyanov Institute of Organoelement Compounds of Russian Academy of Sciences, Vavilova St., 28, bld. 1, Moscow, 119334, Russia

4. Photochemistry Center, FSRC Crystallography and Photonics, Russian Academy of Sciences, Novatorov Str. 7A-1, Moscow, 119421, Russia

\*e-mail: [sosorev@physics.msu.ru](mailto:sosorev@physics.msu.ru)

S1. X-Ray diffraction analysis

**Table S1.** Crystallographic data for NDI-Stb.

|                                      |   |
|--------------------------------------|---|
| Identification code                  | 2240816   |
| Diffractometer                       | Bruker D8 Quest with Photon III detector                      |
| Wavelength, Å                        | 0.71072   |
| Empirical formula                    | C <sub>42</sub> H <sub>26</sub> N <sub>2</sub> O <sub>4</sub> |
| Formula weight                       | 622.65  |
| Temperature, K                       | 122   |
| Crystal system                       | Monoclinic  |
| Space group                          | P2 <sub>1</sub> 2 <sub>1</sub> 2 <sub>1</sub>                 |
| Unit cell dimensions                 |   |
| <i>a</i> (Å)                         | 25.526(6)   |
| <i>b</i> (Å)                         | 5.3037(18)  |
| <i>c</i> (Å)                         | 23.743(6)   |
| <i>b</i>                             | 116.390(9)  |
| Volume                               | 2879.4(14)  |
| Z(Z')                                | 4(0.5)  |
| Density (calculated)                 | 1.436   |
| Absorption coefficient               | 9.71  |
| F(000)                               | 1296  |
| q range for data collection          | 1.91 to 28.995  |
| Reflections collected                | 13613   |
| Independent reflections              | 3816 [R(int) = 0.0796]  |
| Observed reflections                 | 2703  |
| Completeness to q <sub>max</sub> , % | 99.6  |
| Goodness-of-fit on F <sup>2</sup>    | 1.029   |
| Final R indices [I>2σ(I)]            | R1=0.0596, wR2=0.1479   |
| R indices (all data)                 | R1 = 0.0829, wR2 = 0.1677                                     |
| Largest diff. peak and hole          | 0.455 and -0.302 e.Å <sup>-3</sup>                            |

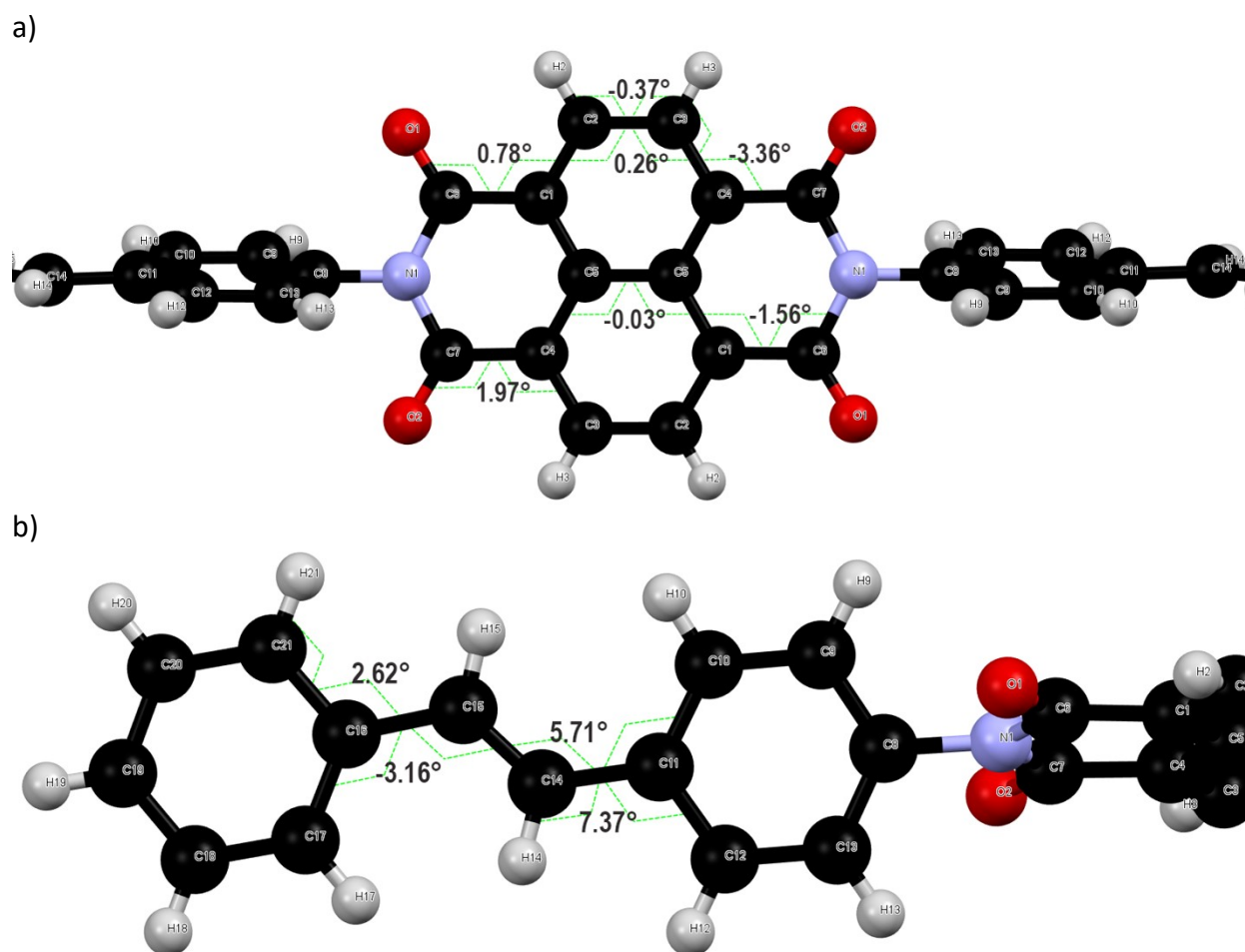


Fig. S1. Molecular structure of NDI-stilbene with labeled atoms and torsion angles for NDI core (a) and stilbene moiety (b).

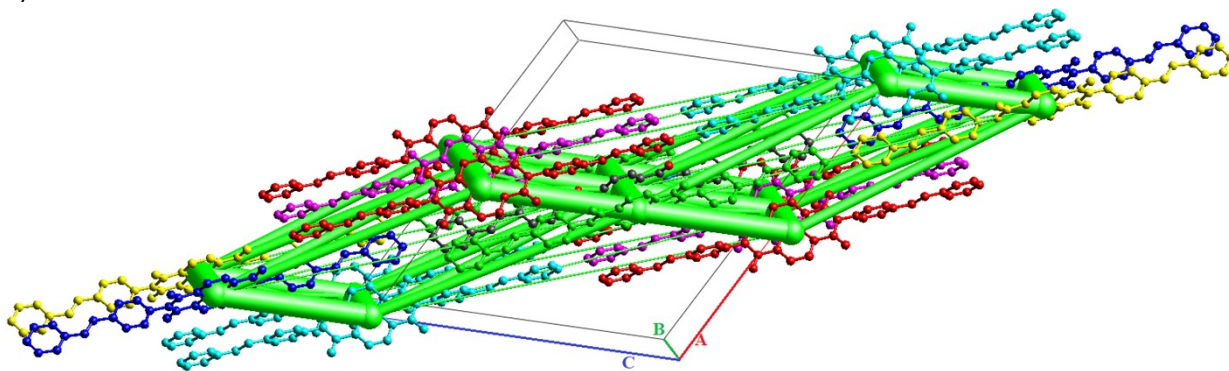
## S2. DFT calculations

Table S2. Energies of the selected molecular orbitals obtained at B3LYP/6-31G(d,p) and CAM-B3LYP/6-31G(d,p) levels.

| Orbital | Energy, eV |        |
|---------|------------|--------|
|         | CAM-B3LYP  | B3LYP  |
| HOMO-10 | -9.200     | -7.502 |
| HOMO-9  | -9.059     | -7.361 |
| HOMO-8  | -8.678     | -7.108 |
| HOMO-7  | -8.667     | -7.091 |
| HOMO-6  | -8.534     | -6.980 |
| HOMO-5  | -8.515     | -6.939 |
| HOMO-4  | -8.357     | -6.857 |
| HOMO-3  | -8.354     | -6.795 |
| HOMO-2  | -8.280     | -6.789 |
| HOMO-1  | -6.988     | -5.573 |
| HOMO    | -6.980     | -5.567 |
| LUMO    | -2.220     | -3.260 |
| LUMO+1  | -0.419     | -1.633 |
| LUMO+2  | -0.310     | -1.467 |
| LUMO+3  | -0.155     | -1.382 |
| LUMO+4  | 0.063      | -1.129 |
| LUMO+5  | 0.495      | -0.873 |
| LUMO+6  | 1.162      | -0.120 |
| LUMO+7  | 1.173      | -0.109 |
| LUMO+8  | 1.317      | 0.0218 |
| LUMO+9  | 1.322      | 0.0272 |

### S3. Energy framework analysis

a)



b)

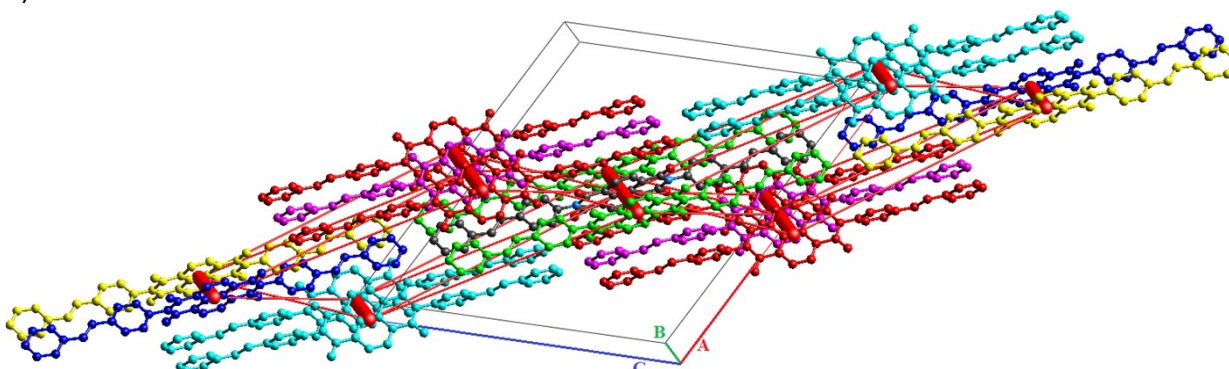


Fig. S2. Graphical representation of the dispersion energy in green on panel (a) and electrostatic interactions on panel (b) in NDI-stilbene crystals. The cylinders link molecular centroids, and their thickness is proportional to the magnitude of the energy; for clarity, pairwise energies with magnitudes less than  $5 \text{ kJ mol}^{-1}$  are not shown. Details are given in Table S1.

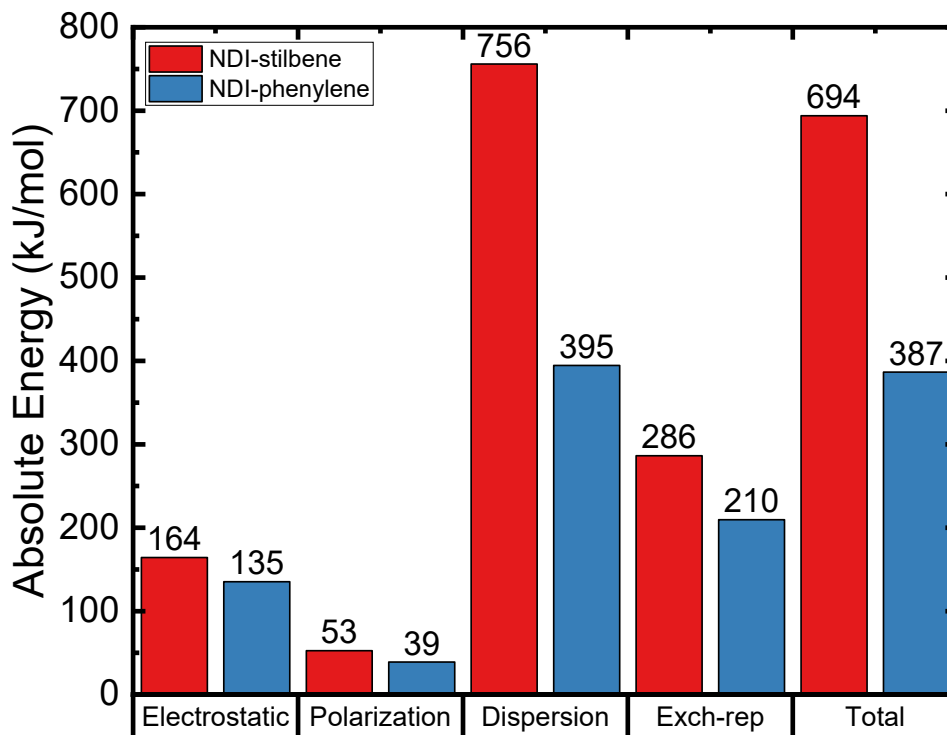


Fig. S3. Distribution of interaction energies (absolute values) of NDI-stilbene and NDI-phenylene for a  $3.8 \text{ \AA}$  cluster. Each energy term was multiplied by the number of corresponding molecular pairs (see fig.3 in the main text).

Table S3. Different interaction energies of the molecular pairs for NDI-stilbene in  $\text{kJ mol}^{-1}$ :  $N$  is the number of pairs,  $R$  is the distance between the molecule centroids,  $E_{\text{ele}}$  is the classical electrostatic energy of interaction between monomer charge distributions,  $E_{\text{pol}}$  is the polarization energy estimated as a sum over atoms with terms of the kind  $-\frac{1}{2}\alpha|F|^2$ , where the electric field  $F$  is computed at each atomic nucleus from the charge distribution of the other monomer and  $\alpha$  are isotropic atomic polarizabilities,  $E_{\text{dis}}$  is Grimme's D2 dispersion correction summed over all intermolecular atom pairs,  $E_{\text{rep}}$  is the exchange–repulsion energy, obtained from the antisymmetric product of the monomer spin orbitals, [1] and  $E_{\text{tot}}$  is the total energy.

|  | $N$ | $R$ (Å) | $E_{\text{ele}}$ | $E_{\text{pol}}$ | $E_{\text{dis}}$ | $E_{\text{rep}}$ | $E_{\text{tot}}$ |
|--|-----|---------|------------------|------------------|------------------|------------------|------------------|
|  | 4   | 13.00   | -7.9             | -3               | -25.7            | 0                | -32.9            |
|  | 2   | 31.67   | -0.6             | -0.3             | -8               | 0                | -7.8             |
|  | 2   | 5.3     | -48.8            | -9.9             | -117.2           | 89.3             | -105.8           |
|  | 4   | 21.11   | -7.4             | -2.5             | -46.2            | 0                | -50              |
|  | 2   | 31.67   | -1.8             | -0.2             | -8.5             | 0                | -9.4             |
|  | 2   | 11.87   | -0.3             | -4.9             | -100.5           | 53.9             | -58.2            |

#### S4. Hirshfeld surface maps

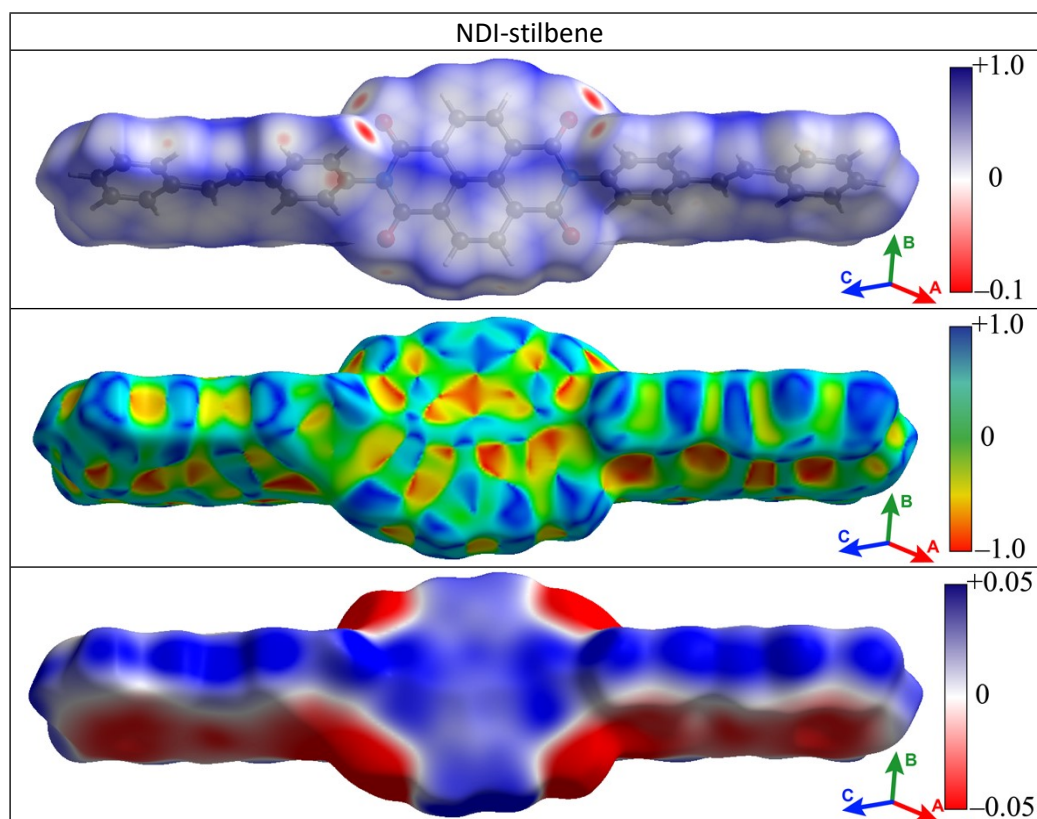


Fig. S4. Hirshfeld surfaces of NDI-stilbene mapped with normalized contact distance (first row), shape index  $S$  (second row), and ESP (third row). Red spots in (a) indicate intermolecular contacts closer than the sum of the van-der-Waals radii (close contacts), blue spots are referred

to longer contacts, and contacts around the sum of van-der-Waals radii (moderate contacts) are white.

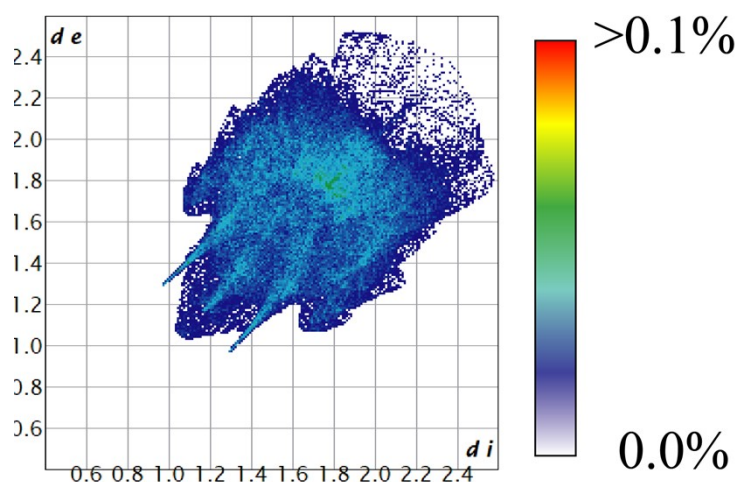


Fig. S5. 2D finger print plot for NDI-stilbene with  $d_i$  and  $d_e$  ranging from 0.5 to 2.9 Å. For any given  $d_i$  and  $d_e$  pairs, the change in color shows the raise in occurrence: white color for no occurrence, then blue green and red for most frequent occurrence.

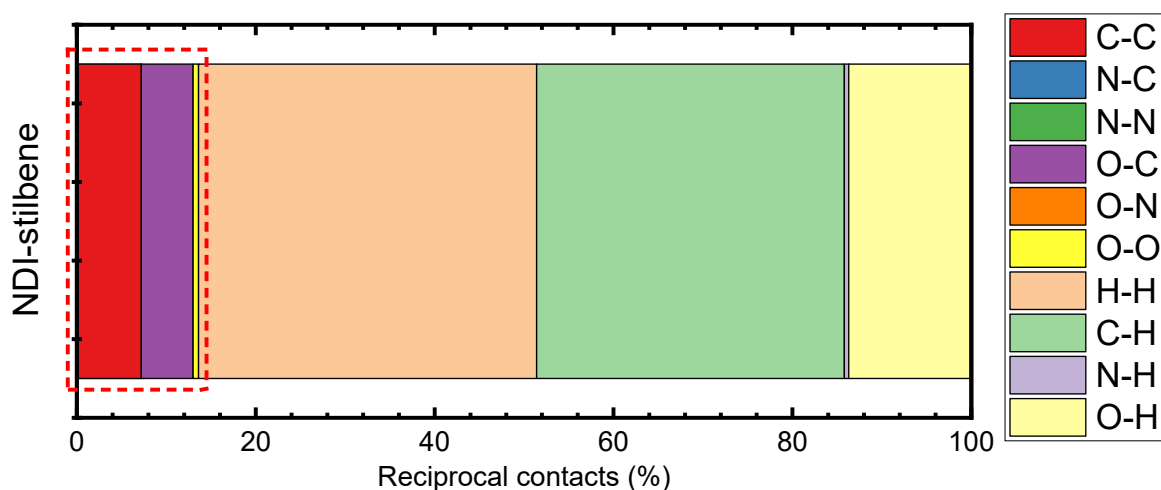


Fig. S6. Distribution of reciprocal intermolecular contacts for NDI-stilbene, arranged by molecules on the basis of Hirshfeld surface analysis. “Conducting” contacts are highlighted with the red dashed frames.

S5. Packing and ESP complementarity

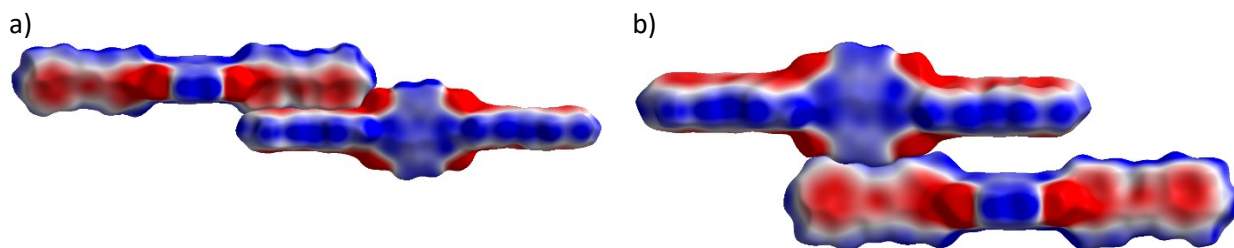


Fig. S7. ESP mapped on the Hirshfeld surfaces of adjacent molecules for the NDI-stilbene crystals. Color mapping and range for ESP correspond to Fig. 7c,d. More information in Ref. [2]. Color mapping and range for ESP correspond to Fig. S4.

## S6. TDDFT calculations

Table S4. Lowest-energy transitions in single molecules of NDI-Stb obtained with B3LYP and CAM-B3LYP functionals.

| #  | B3LYP      |        |   | CAM-B3LYP  |        |   |
|----|------------|--------|---|------------|--------|---|
|    | Energy, eV | f      | Orbitals                                  | Energy, eV | f      | Orbitals                                      |
| 1  | 1.951      | 0.0002 | 98% H – L                                 | 3.511      | 0.0009 | 80% H – L                                     |
| 2  | 1.956      | 0.0002 | 98% H-1 – L                               | 3.523      | 0.0011 | 81% H-1 – L                                   |
| 3  | 3.140      | 0.0001 | 58% H-9 – L<br>31% H-7 - L                | 3.778      | 1.1551 | 89% H-2 - L                                   |
| 4  | 3.177      | 0.0639 | 48% H-4 – L<br>28% H-6 – L<br>21% H-5 - L | 3.981      | 0      | 74% H-10 - L                                  |
| 5  | 3.185      | 0.0181 | 77% H-5 – L<br>10% H-6 – L<br>10% H-4 – L | 4.106      | 0.0378 | 70% H-9 - L                                   |
| 6  | 3.275      | 0.0005 | 42% H-10 – L<br>34% H-8 - L               | 4.118      | 0.0096 | 60% H-11 – L                                  |
| 7  | 3.298      | 0.0000 | 89% H-2 – L                               | 4.303      | 2.0502 | 23% H - L+1<br>25% H – L+2<br>18% H-1 – L+3   |
| 8  | 3.302      | 0.0001 | 89% H-3 – L                               | 4.319      | 0.0328 | 56% H-14 - L                                  |
| 9  | 3.365      | 0.9200 | 56% H-6 – L<br>36% H-4 – L                | 4.335      | 0.0378 | 28% H-1 – L+2<br>15% H – L+2<br>15% H-1 – L+1 |
| 10 | 3.500      | 0.0009 | 58% H-7 – L<br>34% H-9 – L                | 4.473      | 0.0063 | 48% H-5 – L<br>23% H-6 – L                    |
| 11 | 3.519      | 0.0006 | 51% H-8 – L<br>43% H-10 – L               |            |        |   |
| 12 | 3.590      | 0.2068 | 75% H – L+1<br>17% H-1 – L+1              |            |        |   |
| 13 | 3.600      | 0.0168 | 75% H-1 – L+1<br>17% H – L+1              |            |        |   |
| 14 | 3.688      | 0.0001 | 88% H-13 – L                              |            |        |   |
| 15 | 3.746      | 0.0217 | 84% H-11 – L                              |            |        |   |
| 16 | 3.887      | 0.0116 | 90% H-15 - L                              |            |        |   |
| 17 | 3.932      | 1.3270 | 54% H – L+2<br>40% H-1 – L+2              |            |        |   |
| 18 | 3.950      | 0.0447 | 55% H-1 – L+2<br>43% H – L+2              |            |        |   |
| 19 | 3.990      | 0.5946 | 64% H – L+3<br>26% H-1 – L+3              |            |        |   |
| 20 | 4.005      | 0.0253 | 63% H-1 – L+3<br>26% H – L+3              |            |        |   |

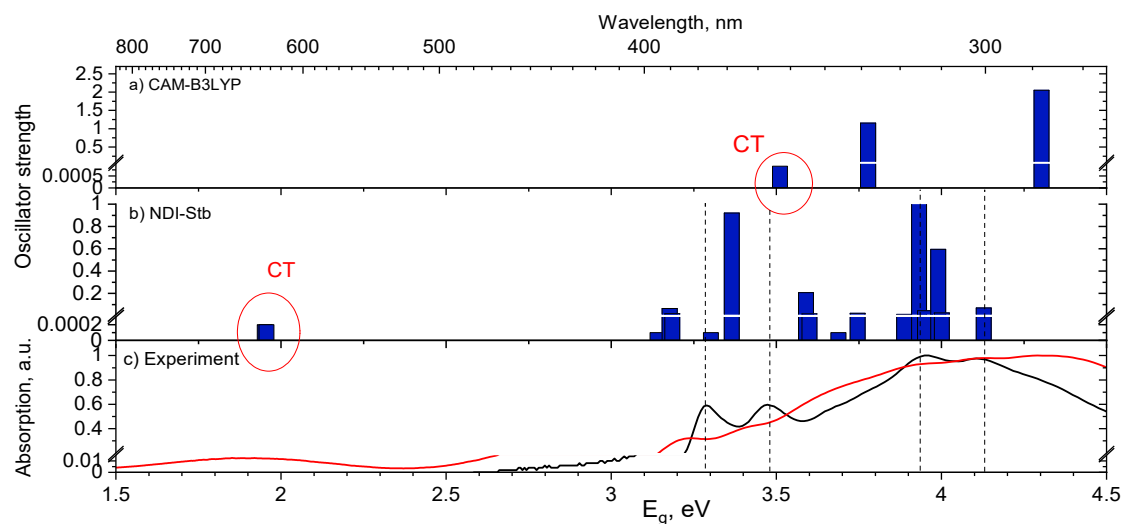


Fig. S8. Comparison of the experimental absorption data for solution (black line) and film (red line) with the ones calculated using B3LYP and CAM-B3LYP functionals.

Table S5. Lowest-energy transitions in CT dimers of NDI-Stb obtained at B3LYP/6-31G(d,p) levels.

| #  | Energy | f      | Transition type (Inter-/intramolecular) |
|----|--------|--------|---|
| 1  | 1.986  | 0.0000 | intermolecular                          |
| 2  | 1.989  | 0.0004 | intramolecular                          |
| 3  | 2.139  | 0.0002 | mostly intramolecular                   |
| 4  | 2.140  | 0.0002 | mostly intramolecular                   |
| 5  | 2.149  | 0.0005 | mostly intermolecular                   |
| 6  | 2.154  | 0.0004 | mostly intermolecular                   |
| 7  | 2.348  | 0.0000 | mostly intermolecular                   |
| 8  | 2.352  | 0.0000 | mostly intermolecular                   |
| 9  | 3.113  | 0.0102 | mostly intermolecular                   |
| 10 | 3.117  | 0.0011 | mostly intramolecular                   |

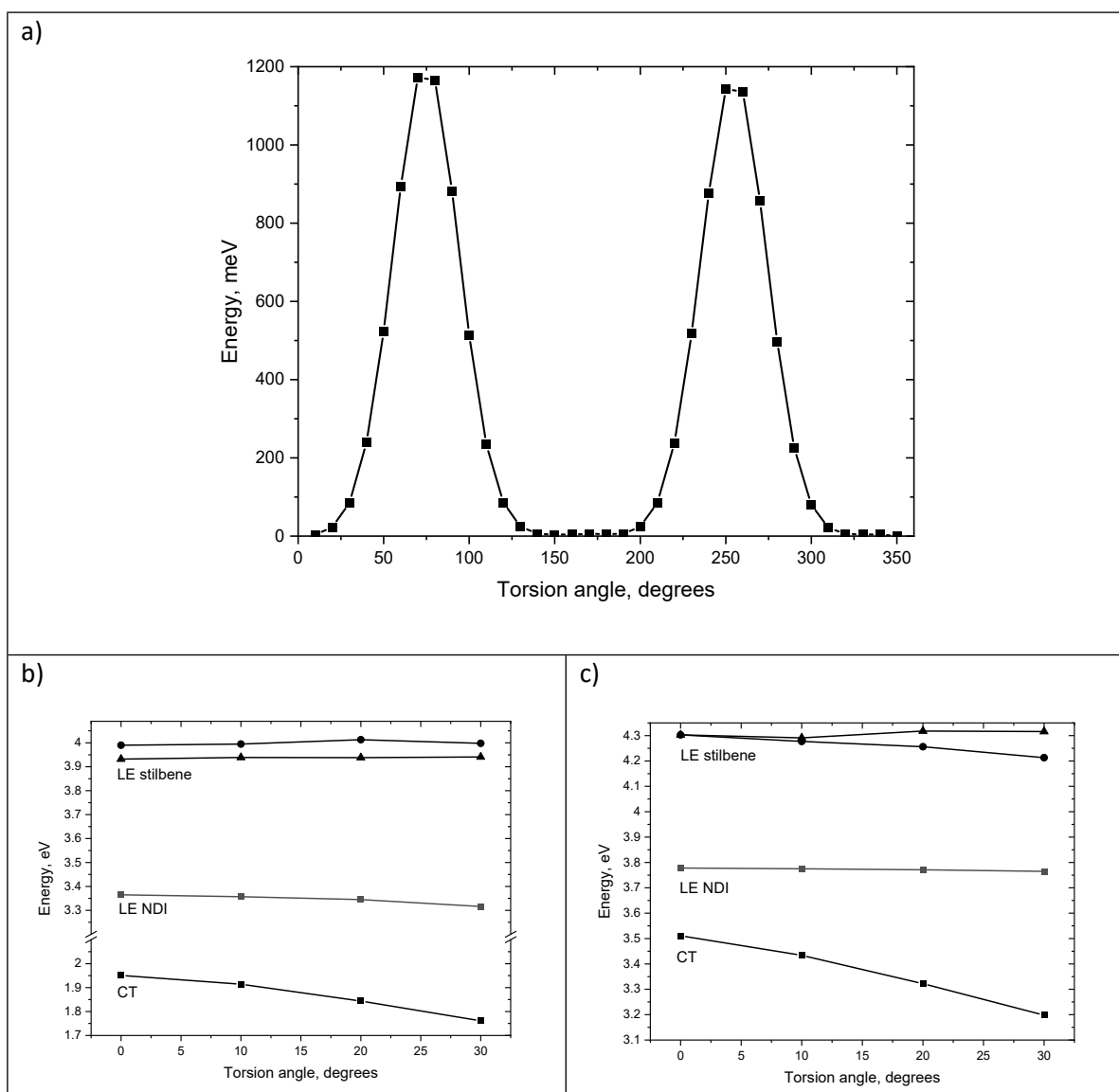


Fig. S9. (a) Energy profile for stilbene torsion with respect to NDI core obtained at CAM-B3LYP/6-31G(d,p) level. (b,c) Energies of the optical transitions for various torsional angles obtained with B3LYP (b) and CAM-B3LYP (c) density functionals. In both panels,  $0^\circ$  corresponds to the equilibrium position.

#### S7. Atomic force microscopy data

a)

b)

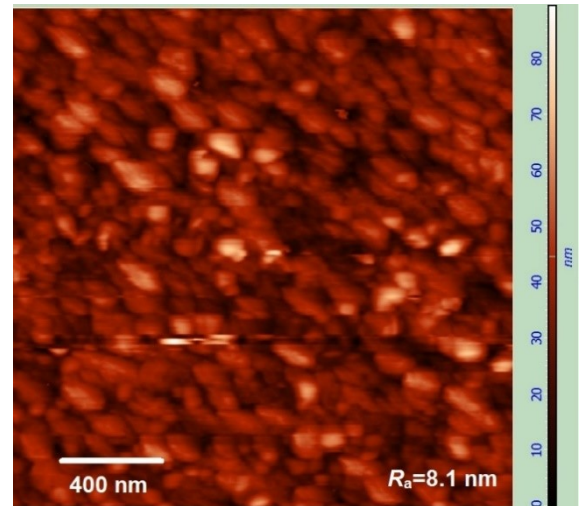
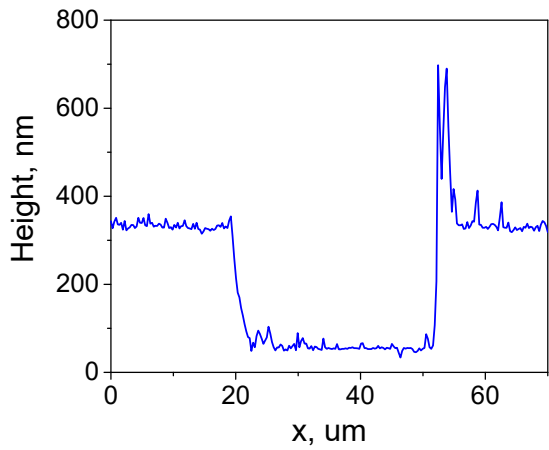
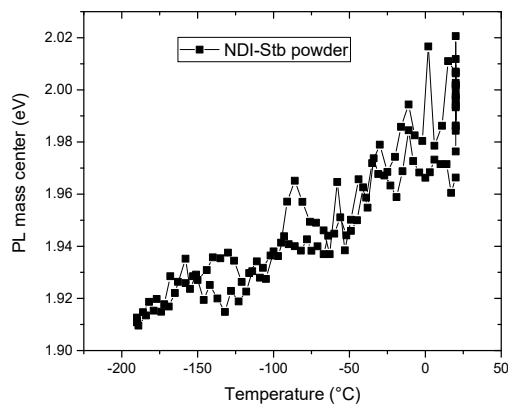


Fig. S10. Atomic force microscopy data for NDI-Stb film: typical scratch profile (a) and 2D surface profile (b). The film thickness was  $291 \pm 15$  nm, and the average roughness was 8.1 nm. The 2D image is a signature of heterogeneous film structure.

### S8. Optical studies

a)



b)

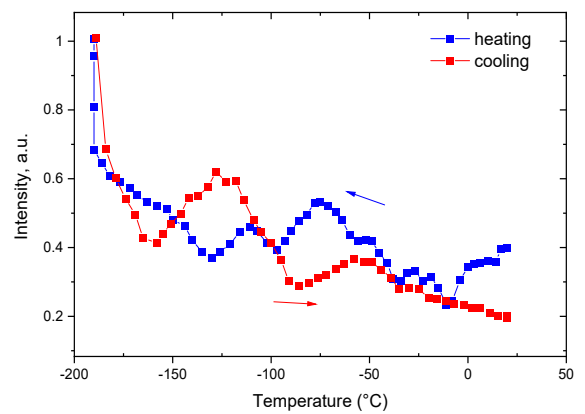


Fig. S11. (a) PL spectrum mass center as a function of temperature. (b) Dependence of PL intensity on temperature for NDI-Stb powder.

S9. Raman spectra calculations

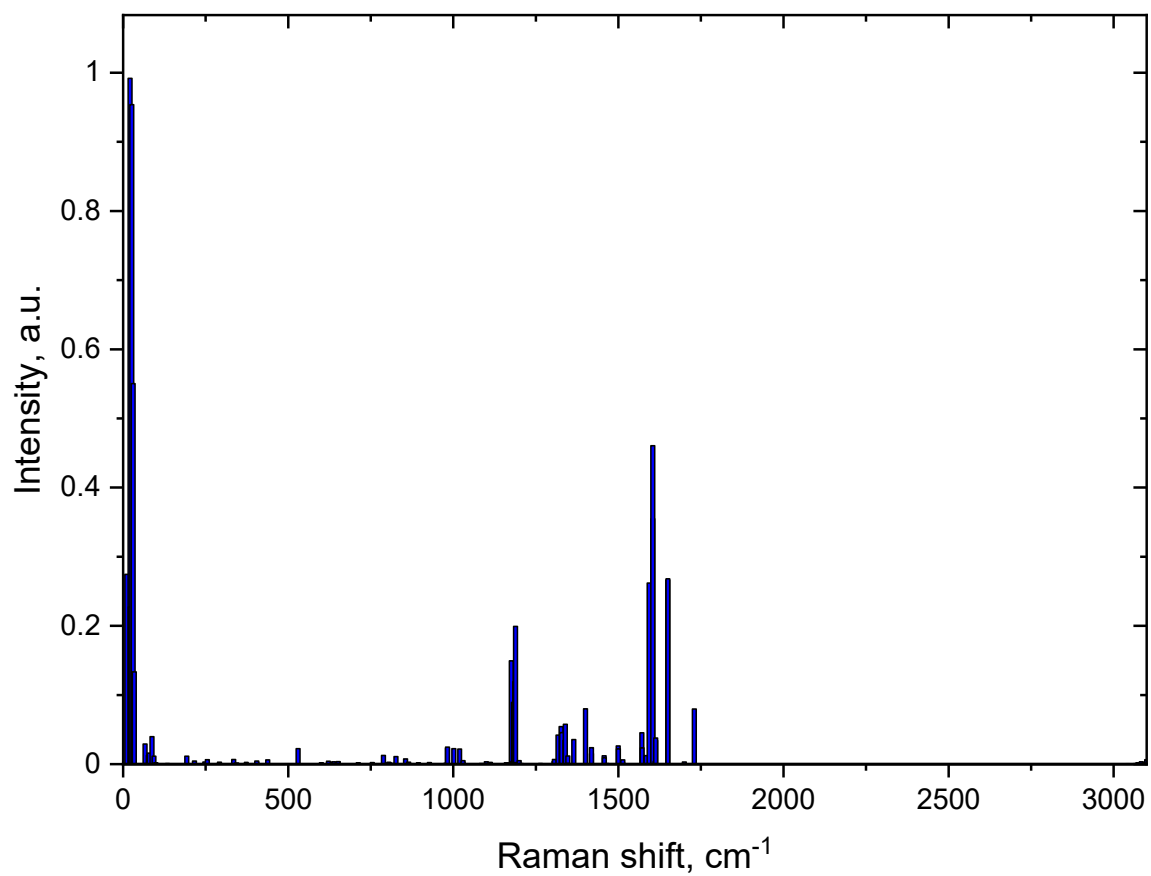
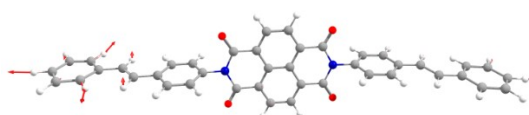


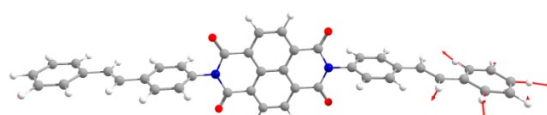
Fig. S12. Calculated Raman spectra for NDI-Stb.

a) band S1

981  $\text{cm}^{-1}$

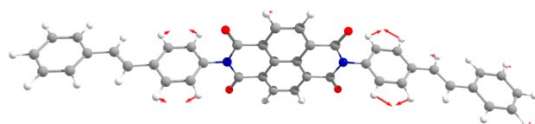


982  $\text{cm}^{-1}$

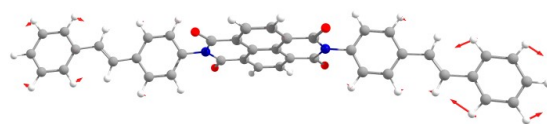


b) band S2

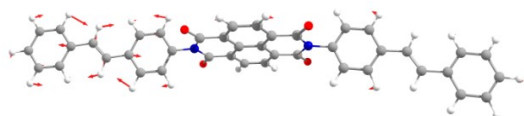
1175  $\text{cm}^{-1}$



1181  $\text{cm}^{-1}$



1189  $\text{cm}^{-1}$



c) band N1

1365  $\text{cm}^{-1}$

1400  $\text{cm}^{-1}$

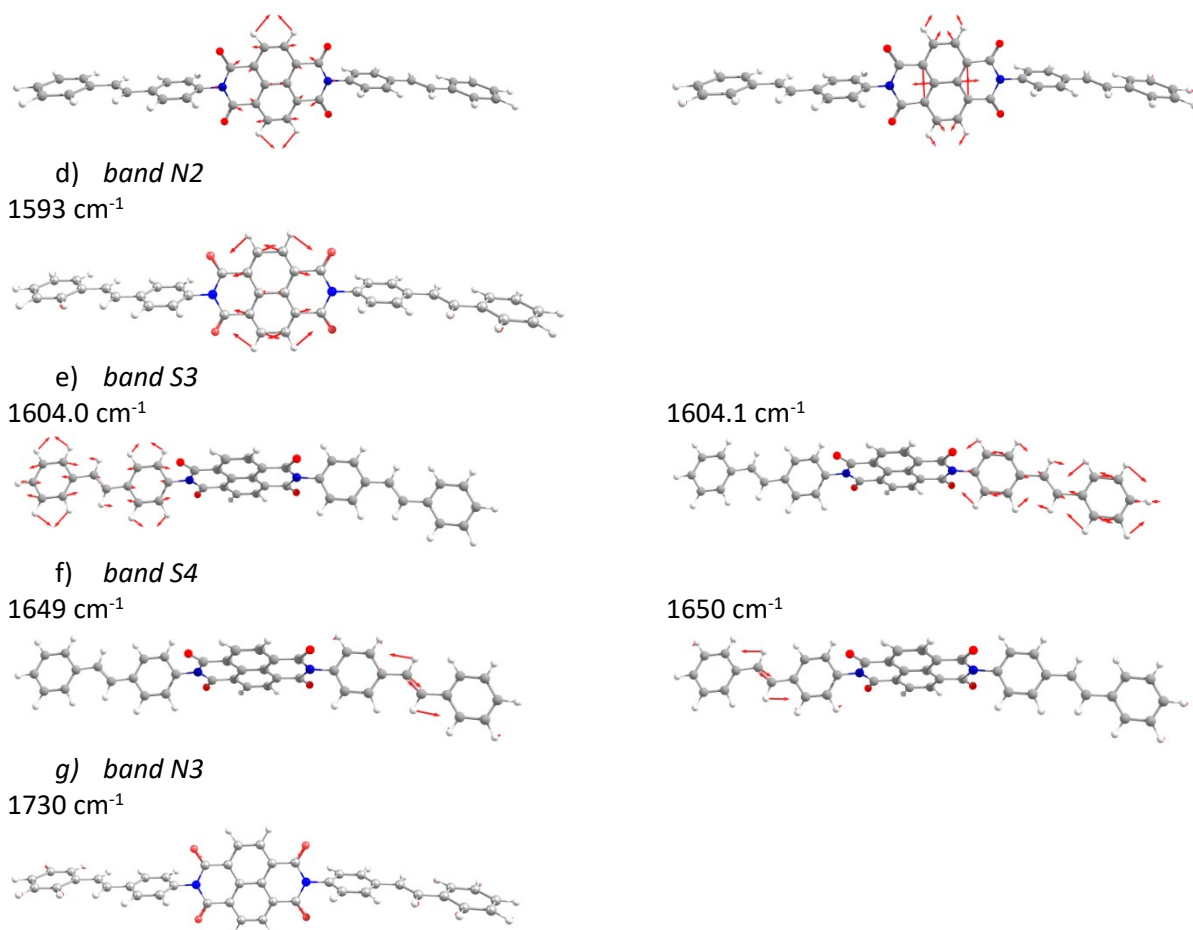


Fig. S13. Calculated atomic displacements for the selected Raman modes. The frequencies are scaled by 0.965.

#### S10. HF Raman spectra

According to Fig. 5, the experimental Raman bands at 998, 1191, 1597, 1639  $\text{cm}^{-1}$  for NDI-stilbene are observed also for stilbene and hence involve vibrations of the latter moieties in the molecule studied. Indeed, our DFT calculations yield that the experimental band at 998  $\text{cm}^{-1}$  (labeled as S1) corresponds to vibrations of terminal (phenyl) ring of stilbene moiety (two modes, see Fig. S10a), band at 1191  $\text{cm}^{-1}$  (S2) — to scissor vibrations of the hydrogens of stilbene phenyl and phenylene rings (three modes, see Fig. S10b), band at 1597  $\text{cm}^{-1}$  (S3) — to stretching of phenyl/phenylene rings and vinylene group (Fig. S10e), and band at 1639  $\text{cm}^{-1}$  (S4) — to stretching vibration of the vinylene group (Fig. S10f). This assignment is in line with the literature data [3, 4]. Band S1 has the same frequency both in stilbene and NDI-stilbene, whereas band S3 is red-shifted with respect to stilbene by 3  $\text{cm}^{-1}$ , respectively. On the contrary, bands S2 and S4 are blue-shifted with respect to stilbene. The relative intensities of bands S1 and S3 drop by  $\sim 3$  and 1.5 times, correspondingly, with respect to those for S2 and S4. We tentatively assign this decrease in the relative intensity to intermolecular interactions present in NDI-Stb crystal, which hinders motion of terminal hydrogen and carbon atoms that contributes significantly to the suppressed modes. In contrast, the motion of the atoms of the phenylene rings (band S2) and vinyl groups (band S4) seem to be not affected by adjacent molecules.

The bands at 1418  $\text{cm}^{-1}$  and 1718  $\text{cm}^{-1}$  of NDI-Stb are assigned to motion of atoms of the NDI core, since almost the same frequencies of the Raman bands are observed in NDI-CHex (at 1425 and 1713  $\text{cm}^{-1}$ , respectively), and labeled as bands N1 and N3. The band at 1606  $\text{cm}^{-1}$  observed in NDI-CHex (N2) probably manifests itself in the spectrum of NDI-stilbene as a shoulder of the band at 1597  $\text{cm}^{-1}$ . The relative

intensity of band N1 in the NDI-Stb spectrum is lower than in the NDI-CHex spectrum, which can be assigned to stronger interaction of side carbon and hydrogen atoms lowering their vibrational amplitude.

#### S11. LF Raman spectra of the film

LF Raman spectrum is very sensitive to the intermolecular interactions and packing and can be used for investigation of the film crystallinity and polymorphism [Brillante]. For this reason, we performed LF Raman measurements for NDI-Stb film and compared the results obtained to those for the polycrystalline powder. The LF Raman spectra for the film is collated to that for crystalline powder in Fig. S. ... In contrast to the data for crystalline powder, LF spectra for the NDI-Stb film contain broad low-frequency band and does not show prominent characteristic peaks. This is frequently observed in amorphous samples, in line with our suggestion that the film has considerable amorphous areas.

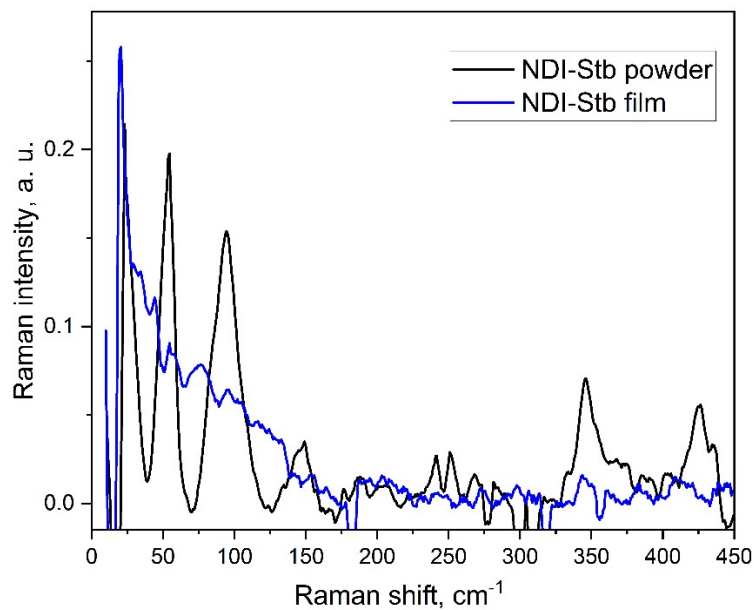


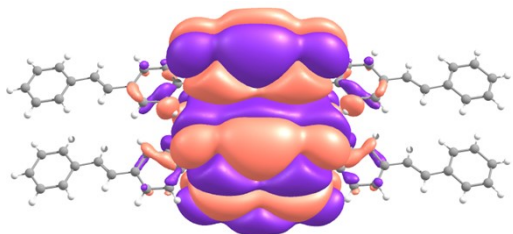
Fig. S14. Low-frequency Raman spectra for NDI-Stb powder and film.

S12. Charge mobility calculations

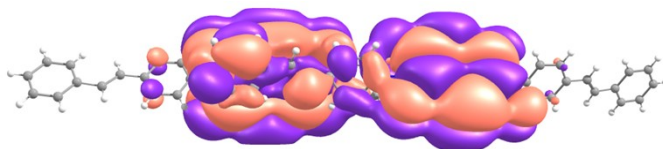
Table S6. Charge transfer integral values for various directions in NDI-Stb.

| dimer | r, Å  | V <sub>h</sub> , eV | V <sub>l</sub> , eV |
|-------|-------|---------------------|---------------------|
| 1     | 5.33  | 0.026               | -0.064              |
| 2     | 5.33  | 0.027               | -0.064              |
| 3     | 11.93 | -0.004              | -0.001              |
| 4     | 11.93 | 0.006               | -0.002              |
| 5     | 31.83 | 0.011               | -0.000              |
| 6     | 31.83 | 0.001               | -0.000              |
| 7     | 31.83 | -0.004              | 0.000               |

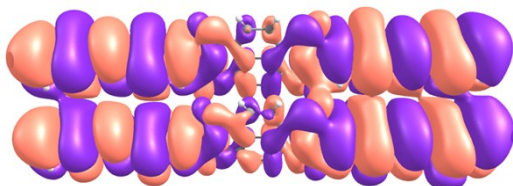
a) LUMO,  $\pi$ -stacking direction



b) LUMO, CT direction



c) HOMO,  $\pi$ -stacking direction



d) HOMO, CT direction

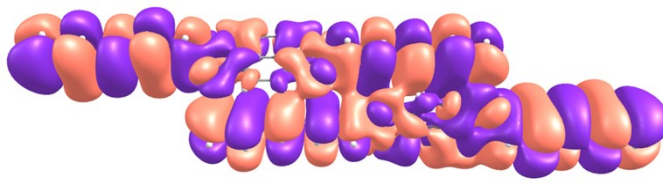
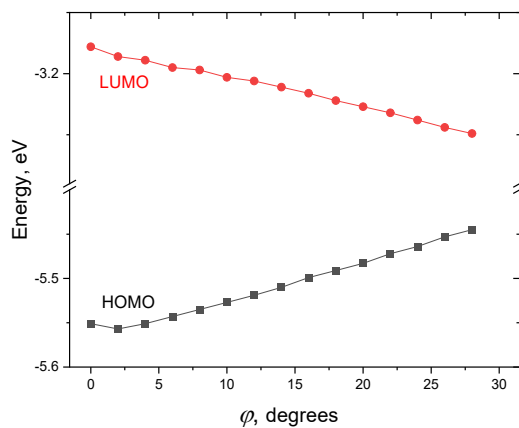


Fig. S15. HOMO (a,b) and LUMO (c,d) of molecular dimers corresponding to  $\pi$ -stack (a, c) and CT direction (b, d).

a)



b)

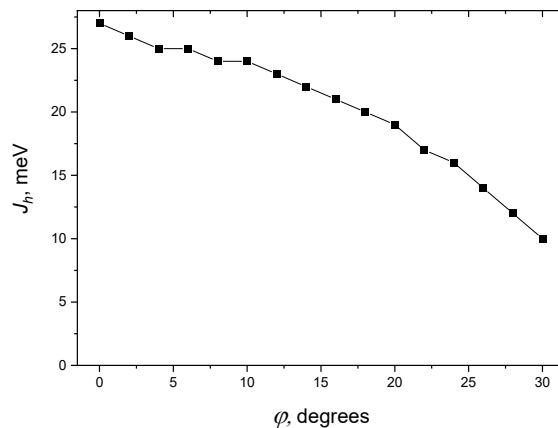


Fig. S16. HOMO and LUMO energies (a) and hole transfer integrals (b) as a function of torsional angle

between stilbene and NDI moieties obtained at B3LYP/6-31G(d,p) level. In both panels, 0° corresponds to the equilibrium position.

### S13. Charge mobility measurements

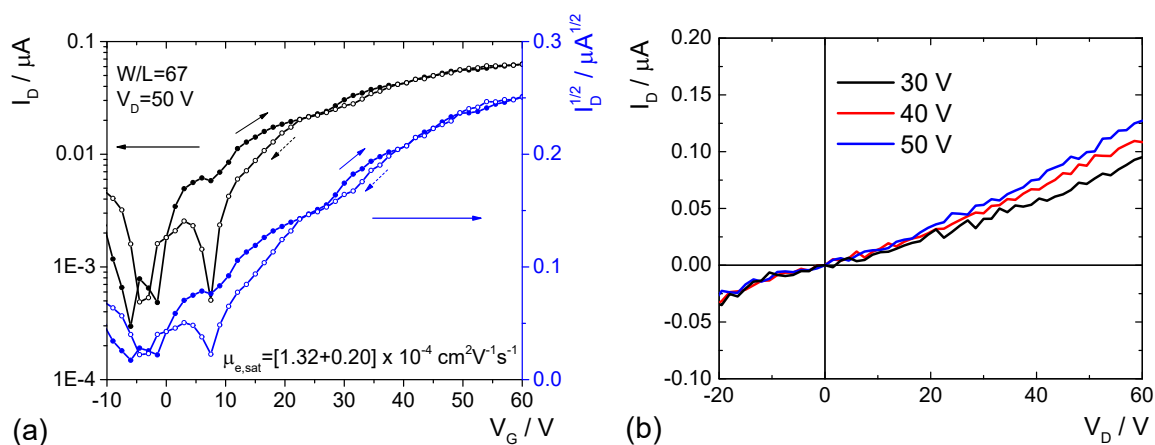


Fig. S17. Typical transfer (a) and output (b) characteristics of NDI-Stb based OFETs.

### References

1. Mackenzie C. F., Spackman P. R., Jayatilaka D., Spackman M. A. CrystalExplorer model energies and energy frameworks: extension to metal coordination compounds, organic salts, solvates and open-shell systems. *IUCr*. 2017. № 5. C. 575–7. <https://dx.doi.org/10.1107/S205225251700848X>.
2. Edwards A. J., Mackenzie C. F., Spackman P. R., Jayatilaka D., Spackman M. A. Intermolecular interactions in molecular crystals: what's in a name? *Faraday Discuss.* 2017;203:93-112. <https://dx.doi.org/10.1039/C7FD00072C>.
3. Meic Z., Gusten H. Vibrational studies of trans-stilbenes – I. Infrared and Raman spectra of trans-stilbene and deuterated stilbenes. *Spectrochimica Acta* 1978; 34A: 101-11.
4. Vintaykin I. B., Golyak II. S., Golyak Ig. S., Esakov A.A., Morozov A.N., Tabalin S.E. The Use of Raman Spectroscopy for the Rapid Analysis of Chemical Compounds. *Russian Journal of Physical Chemistry B*, 2020, Vol. 14, No. 5, pp. 752–9. <https://doi.org/10.1134/S1990793120050255>